Detection of cholesterol bilayer domains in intact biological membranes: Methodology development and its application to studies of eye lens fiber cell plasma membranes

Laxman Mainali[a], **William J. O'Brien**[b], and **Witold K. Subczynski**[a,*]

[a]Department of Biophysics, Medical College of Wisconsin, Milwaukee, USA

[b]Department of Ophthalmology and Visual Science, Eye Institute, Medical College of Wisconsin, Milwaukee, USA

Abstract

Four purported lipid domains are expected in plasma membranes of the eye lens fiber cells. Three of these domains, namely, bulk, boundary, and trapped lipids, have been detected. The cholesterol bilayer domain (CBD), which has been detected in lens lipid membranes prepared from the total lipids extracted from fiber cell plasma membranes, has not yet been detected in intact fiber cell plasma membranes. Here, a saturation-recovery electron paramagnetic resonance spin-labeling method has been developed that allows identification of CBDs in intact fiber cell plasma membranes of eye lenses. This method is based on saturation-recovery signal measurements of the cholesterol-analog spin label located in the lipid bilayer portion of intact fiber cell membranes as a function of the partial pressure of molecular oxygen with which the samples are equilibrated. The capabilities and limitations of this method are illustrated for intact cortical and nuclear fiber cell plasma membranes from porcine eye lenses where CBDs were detected in porcine nuclear intact membranes for which CBDs were also detected in lens lipid membranes. CBDs were not detected in porcine cortical intact and lens lipid membranes. CBDs were detected in intact membranes isolated from both cortical and nuclear fiber cells of lenses obtained from human donors. The cholesterol content in fiber cell membranes of these donors was always high enough to induce the formation of CBDs in cortical as well as nuclear lens lipid membranes. The results obtained for intact membranes, when combined with those obtained for lens lipid membranes, advance our understanding of the role of high cholesterol content and CBDs in lens biology, aging, and/or cataract formation.

Keywords

---

*Corresponding Author: Witold K. Subczynski, Department of Biophysics, Medical College of Wisconsin, 8701 Watertown Plank Road, Milwaukee, WI 53226, USA, Tel: (414) 955-4038; Fax: (414) 955-6512; subczyn@mcw.edu.

1.   Introduction

Four types of lipid domains are likely to exist in the lipid bilayer portion of intact membranes of the eye lens fiber cells, which are loaded with integral membrane proteins (Bassnett et al., 2011; Gonen et al., 2004; Gonen et al., 2005; Kistler and Bullivant, 1980; Li et al., 1986) and with high cholesterol (Chol) content (Borchman et al., 1989; Cenedella, 1996; Jacob et al., 1999; Li et al., 1985, 1987; Mainali et al., 2017b; Rujoi et al., 2003; Zelenka, 1984) (Fig. 1B). Domains include the bulk lipid domain, boundary lipid domain, trapped lipid domain, and pure Chol bilayer domain (CBD) (Mainali et al., 2012; Raguz et al., 2014, 2015c; Subczynski et al., 2017). The bulk lipid domain is formed by a liquid-ordered-phase bilayer that contains lipids nearly unaffected by the presence of membrane proteins (Mainali et al., 2012). Boundary and trapped lipid domains are formed in the presence of integral membrane proteins. The boundary lipid domain contains lipids in contact with protein and bulk lipids. The exchange rate between boundary and bulk lipids is of the order of magnitude of 10^7 s^{-1} or greater (East et al., 1985; Marsh, 1997; Ryba et al., 1987). The trapped lipid domain is formed by lipids in contact with two proteins and/or by lipids in contact with proteins and boundary lipids. The exchange rate with other domains is of the order of magnitude of 10^5 s^{-1} or less (Kawasaki et al., 2001).

The CBD is a highly fluid, pure Chol bilayer surrounded by the bulk lipid domain formed by phospholipids (PLs) saturated with Chol (Mainali et al., 2013b; Plesnar et al., 2013; Raguz et al., 2011a, b). This domain was detected in lens lipid membranes (LLMs) with high Chol content (Mainali et al., 2012, 2013a, 2015; Raguz et al., 2009) (Fig. 1D). It should be noted that the CBD, which is the major subject of this paper, is different from the raft domain. The former is a pure Chol bilayer immersed in the bulk PL-Chol membrane (Litz et al., 2016; Plesnar et al., 2013; Raguz et al., 2015a; Raguz et al., 2011a, b) (PL bilayer saturated with Chol, which is in the liquid-ordered phase (Plesnar et al., 2013)). The latter is formed by a mixture of PLs (mainly sphingolipids) containing ~33 mol% Chol (de Almeida et al., 2003; Rog and Vattulainen, 2014; Veatch and Keller, 2003). Raft is a liquid-ordered-phase domain immersed in the liquiddisordered bulk membrane (Edidin, 2003; Simons and Vaz, 2004).

In our previous works, we applied electron paramagnetic resonance (EPR) spin-labeling methods to discriminate lipid domains in intact fiber cell plasma membranes prepared from human (Raguz et al., 2014, 2015c) and animal (Mainali et al., 2012) eye lenses. We could discriminate three of these purported domains, namely, bulk, boundary, and trapped lipids. However, we were not able to show the presence of CBDs in intact membranes, despite the fact that they were clearly detected in human (Mainali et al., 2013a, 2015, 2017b) and animal (Mainali et al., 2012; Raguz et al., 2009) LLMs. Here, we tested the hypothesis that whenever CBDs are detected in LLMs (Fig. 1D), they also exist in intact lens membranes (Fig. 1B). To achieve that goal, we modified a saturation-recovery (SR) EPR method that we previously developed (named the discrimination by oxygen transport [DOT] method) (Ashikawa et al., 1994).

1.1.   Outline of theory for discriminating CBDs in intact membranes

The CBD was successfully detected in model membranes (Mainali et al., 2013b; Raguz et al., 2011a, b) and LLMs (Mainali et al., 2012, 2013a, 2015, 2017b; Raguz et al., 2009) using

the DOT method. The DOT method is a dual-probe SR EPR approach, in which the observable parameter is the spin-lattice relaxation time (T_1) of lipid spin labels, and the measured value is the bimolecular collision rate between molecular oxygen and the nitroxide moiety of spin labels. This method was introduced by Ashikawa et al. (Ashikawa et al., 1994) and successfully applied for the discrimination of two coexisting domains (Subczynski et al., 2007). The spin label alone usually could not differentiate between these domains (T_1 values are too close). This also is the case with the discrimination of CBDs in model membranes. Because CBDs are pure Chol bilayers, they can be discriminated from the surrounding domain (BULK domain) using the DOT method with the Chol analog spin label (ASL, see (Mainali et al., 2013b; Raguz et al., 2011a, b) for more details). However, in the absence of oxygen, the SR signal is a single-exponential curve with the time constant of T_1(N$_2$, BULK+CBD). In membranes equilibrated with air, the molecular oxygen—through bimolecular collisions with nitroxides induces spin exchange—leads to faster spin-lattice relaxation of nitroxides. An oxygen transport parameter (OTP), W(x), is used as a convenient quantitative measure of the collision rate between the spin label and molecular oxygen (Kusumi et al., 1982):

$$W(\text{x}) = T_1^{-1}(\text{Air, x}) - T_1^{-1}(\text{N}_2,\ \text{x}) = AD(\text{x})C(\text{x}) \quad (1)$$

W(x) is normalized to the sample equilibrated with air and is proportional to the product of the translational diffusion coefficient, D(x), and the concentration, C(x), of oxygen at location "x" in the membrane.

The oxygen partitioning and oxygen diffusion in coexisting lipid domains are affected by lipid packing in these domains. This can be easily observed by recording, in the presence of oxygen, the different T_1s of spin labels located in these two domains. Thus, in the case of the CBD immersed in the bulk PL bilayer, the SR signal observed for membranes equilibrated with air will be a double-exponential curve with time constants of T_1(Air, BULK) and T_1(Air, CBD). The two values of the oxygen transport parameter, which differentiate these domains, can be calculated as follows:

$$W(\text{BULK}) = T_1^{-1}(\text{Air, BULK}) - T_1^{-1}(\text{N}_2,\ \text{BULK} + \text{CBD}) \quad (2)$$

$$W(\text{CBD}) = T_1^{-1}(\text{Air, CBD}) - T_1^{-1}(\text{N}_2,\ \text{BULK} + \text{CBD}) \quad (3)$$

This procedure for processing data from the fitted SR signals from ASL in model membranes and LLMs containing the CBD to the double-exponential curve is schematically illustrated in Fig. 2A.

Why, then, is it that the DOT method cannot discriminate the CBD in intact lens membranes, despite the fact that CBDs are clearly detected in LLMs? The DOT method has been used thus far to distinguish two domains of similar fluidity but with different oxygen solubility

and diffusion. Work described in this paper is the first extension of the DOT method to more complex systems. As indicated above, intact membranes contain four purported domains, two of which are induced by the presence of integral membrane proteins (boundary and trapped lipids), and two of which are formed due to the presence of high Chol (bulk and CBD). The CBD can be detected only with the use of the Chol analog spin label, ASL, which, similar to Chol, can be located in only three of these purported domains, namely, bulk, CBD, and trapped lipids. Literature (Bieri and Wallach, 1975; Warren et al., 1975), as well as our own observations (Mainali et al., 2012; Raguz et al., 2014, 2015c), indicates that Chol (and ASL) is substantially excluded from the boundary lipids. In intact fiber cell membranes in the absence of oxygen, the SR signal coming from ASL can be fitted only by a double-exponential curve with a short- and a long-time constant. The short T_1 is close to that observed for LLM and was assigned as coming from the unresolved bulk plus CBD domain (T_1(N$_2$, BULK+CBD)). The long T_1 was assigned as coming from ASL located in the trapped lipid domain (T_1(N$_2$, TRAP)). We expected that the DOT method would allow detection of the CBD by fitting the SR signal coming from ASL in intact membranes equilibrated with air by a triple-exponential curve with time constants T_1(Air, BULK), T_1(Air, CBD), and T_1(Air, TRAP). However, we encountered the problem that the triple exponential model was too simplistic to describe the heterogeneous intact membrane environment. We were able to fit the SR signal to a double-exponential curve with time constants T_1(Air, BULK+CBD) and T_1(Air, TRAP). The two calculated values of the OTP characterize unresolved (apparent) OTP in the bulk plus CBD domain and in the trapped lipid domain,

$$W(\text{BULK} + \text{CBD}) = T_1^{-1}(\text{Air, BULK} + \text{CBD}) - T_1^{-1}(\text{N}_2, \text{ BULK} + \text{CBD}) \quad (4)$$

$$W(\text{TRAP}) = T_1^{-1}(\text{Air, TRAP}) - T_1^{-1}(\text{N}_2, \text{ TRAP}). \quad (5)$$

This procedure for processing the data obtained from fitting the SR signals from ASL in intact membranes to the double-exponential curve is schematically illustrated in Fig. 2B.

To solve our problem, we applied an approach that we have used previously (Mainali et al., 2017a), allowing us to reliably fit SR signals to triple exponentials by fixing some of the time constants. Here, we fixed T_1(Air, TRAP)* (obtained from fitting the SR signal to a double exponential curve) and again fitted the SR signal to triple exponentials with the now fixed time constant. This approach allowed separation of two remaining time constants, namely T_1(Air, BULK) and T_1(Air, CBD). Using these time constants, we were able to calculate OTP values sensed by the ASL in bulk, CBD, and trapped lipid domains,

$$W(\text{BULK}) = T_1^{-1}(\text{Air, BULK}) - T_1^{-1}(\text{N}_2, \text{ BULK} + \text{CBD}) \quad (6)$$

$$W(\text{CBD}) = T_1^{-1}(\text{Air, CBD}) - T_1^{-1}(\text{N}_2, \text{ BULK} + \text{CBD}) \quad (7)$$

$$W(\text{TRAP})^* = T_1^{-1}(\text{Air, TRAP})^* - T_1^{-1}(\text{N}_2, \text{ TRAP})^*. \quad (8)$$

This procedure for processing the data from the fitted SR signals from ASL in intact membranes to triple-exponential curves is schematically illustrated in Fig. 2C.

2.   Materials and Methods

2.1.   Materials

The spin-label cholesterol analogue (androstane spin label [ASL]) was purchased from Molecular Probes (Eugene, OR). Other chemicals, of at least reagent grade, were purchased from Sigma-Aldrich (St. Louis, MO). The ASL chemical structure and its approximate location in the lipid bilayer is schematically illustrated in Fig. 1 in (Raguz et al., 2015b).

2.2.   Isolation and spin labeling of intact and LLMs

The procedures used here are the same as those described previously for intact (Mainali et al., 2012; Raguz et al., 2014) and LLMs (Mainali et al., 2013a). Cortical and nuclear intact and LLMs were isolated separately from six sets of porcine lenses from two-year-old animals (four lenses in each set). Intact cortical and nuclear membranes were also isolated separately from the tissue of single transparent human lenses (from the left and the right eyes) from donors of different ages (40, 46, and 53 years old). As discussed previously, spin-labeled membrane suspensions were transferred to a 0.6 mm inner diameter capillary made of gas-permeable methylpentene polymer (TPX) and used for SR EPR measurements (Subczynski et al., 2005).

2.3.   SR measurements

To further increase the signal-to-noise ratio, samples in TPX capillaries were centrifuged as described in (Subczynski et al., 2005). Samples were equilibrated directly in the resonator with nitrogen or an air/nitrogen mixture. This gas was also used for temperature control. All measurements were carried out at 37°C. SR EPR signals were obtained by short-pulse (300 ns) experiments with 10^5–10^6 decays acquired with 2,048 data points on each signal (decay). Measurements were performed at X-band on a home-built spectrometer with recent major hardware improvements and equipped with a loop-gap resonator (LGR) (Mainali et al., 2017a). These improvements were essential to obtaining reliable SR signals with double- and triple-exponential content. However, problems were encountered during straightforward fitting of the SR signals coming from heterogeneous intact fiber cell membranes labeled with ASL to triple exponentials. In the investigated intact eye lens membranes, ASL can be located in three purported domains, bulk lipids, CBD, and trapped lipids (see Fig. 1B); in the presence of oxygen, we expected to obtain a triple-exponential SR signal. One component of this signal should come from the ASL located in the trapped lipid domain. The trapped lipid

domain is easily discriminated also in deoxygenated samples with $T_1^{-1}(\text{N}_2, \text{ TRAP})$ and is clearly separated from the unresolved bulk plus CBD component with $T_1^{-1}(\text{N}_2, \text{ BULK + CBD})$ (see Fig. 2B). Thus, as follows from Eq. (1), in the presence of oxygen, the spin-lattice relaxation rate of ASL in the trapped lipid domain equals $T_1^{-1}(\text{O}_2, \text{ TRAP}) = T_1^{-1}(\text{N}_2, \text{ TRAP}) + AD(\text{TRAP})C(\text{TRAP})$ (see Fig. 2B). In the strategy developed here, the tail of the SR signal was first fitted to a two-exponential model. The longest time constant coming from the trapped lipid domain ($T_1^{-1}(\text{N}_2, \text{ TRAP})$* or $T_1^{-1}(\text{O}_2, \text{ TRAP})$*) was fixed (see. Fig. 2C). The SR signal was again fitted to the triple exponential, now with one fixed time constant.

The uncertainties in the measurements of decay time from the fits were usually less than 5% for double-exponential fits and less than 14% and 24% for longer and shorter components, respectively, in triple-exponential fits. When necessary, the continuous wave EPR spectra were recorded with a Bruker EMX spectrometer.

2.4. Optimization of spectrometer and recording conditions

In the previous paper (Mainali et al., 2017a), we described an optimization process for similar samples (intact cortical and nuclear fiber cell membranes isolated from two-year-old porcine and containing ASL) for deoxygenated conditions. Here, we used a similar optimization process for samples equilibrated with 30% and 50% air. SR signals in our samples have two or three components; therefore, we performed short-pulse experiments that allowed better separation of components but did not affect the obtained T_1 values. These were qualitative experiments that allowed determination of relevant T_1 values and did not require pump power to be a saturating power for all SR signal components. We used the maximal available pump power, namely +30 dBm (1 W). However, for qualitative experiments, the observing power should be small enough that it will not induce an artefactual shortening of T_1s. For all experiments, the observing power was set to −12 dBm. It should be noted that the nonuniformity of the radio frequency magnetic field over the sample should be avoided for qualitative and quantitative SR experiments. In the future, we will use those from the new class of the uniform field LGRs that satisfy these requirements (Mett et al., 2007; Sidabras et al., 2017).

The SR spectrometer improvements allowed the receiver delay time to be decreased to 100 ns, which increased the accuracy of measurements for samples with short T_1s. (This is the case for samples equilibrated with air.) However, to ensure a reliable fit for data containing double or triple exponentials, additional points must be removed from the dataset post-acquisition. In the strategy applied here, a double-exponential fit was performed first. The number of beginning points removed was increased until the long time component T_1 value obtained from the fitting converged to the constant value independent of further point removal. This indicated that all processes that shortened the long time constant had ended. Based on these results, we concluded that this T_1 is a characteristic of the investigated system (ASL in trapped lipid domain) and that it characterizes the relaxation process of the ASL in trapped lipids after the end of the saturating pulse (independent of the number of

points cut). Thus, this T_1 value can be fixed, allowing SR signals to be fitted to triple exponentials just after the end of the delay time.

This optimization was performed for deoxygenated samples and samples equilibrated with 30% and 50% air. The reliable fits for deoxygenated samples and samples equilibrated with air were obtained by removing, on average, 30 points and 60 points, respectively, from the beginning of the 2048 dataset. (The beginning of the recording always contains some unpredictable processes connected with switches.) In all measurements, sample intervals of 20 ns and 10 ns were used for deoxygenated samples and for samples equilibrated with air, respectively.

2.4. Statistical analysis

For the statistical analysis, results for six independently obtained cortical and six independently obtained nuclear membrane samples were compared. Mean measured values and standard deviations were calculated. The Student's t-test was used to determine the significance of experimental differences. P 0.05 was considered to be statistically significant.

3. Results and Discussion

3.1. Development of the method: experiments with porcine intact fiber cell plasma membranes

This work had two major goals. First, we wanted to modify the available method used for discrimination of the CBD in LLM to the stage that can also allow discrimination of the CBD in intact fiber cell membranes. The second goal was to test our hypothesis that the CBD exists in intact lens membranes when it is detected in LLMs. To demonstrate how the method, which was described in theory in Sect. 1.1, actually works in real systems, we chose cortical and nuclear fiber cell membranes isolated from two-year-old porcine lenses. We previously investigated these intact membranes as well as LLMs prepared from the total lipid extracts from these intact membranes (Mainali et al., 2011; Mainali et al., 2012). As was shown, the CBDs were not detected in porcine cortical LLMs because the Chol content in these membranes is too low (Fig. 1C). In porcine nuclear LLMs, the Chol content is significantly greater, which ensures the formation of CBDs (Fig. 1D). As expected, SR signals in the absence and presence of oxygen for ASL in cortical LLMs were satisfactorily fitted only to single-exponential curves (data not shown). However, for nuclear LLMs, the data were satisfactorily fitted to single exponential curves in the absence of oxygen and to double exponential curves in the presence of oxygen (data not shown). These data (illustrated schematically in Fig. 2A) indicate that two-year-old porcine CBDs are present only in nuclear LLMs.

The straightforward application of the DOT method to discriminate purported CBD domains in intact porcine cortical and nuclear membranes was not successful. This approach is illustrated schematically in Fig. 2B. For deoxygenated samples, SR signals for cortical and nuclear intact membranes were successfully fitted to double-exponential curves (see data for 0% air in Figs. 3B and 4B). As indicated in Sect. 1.1, the long T_1 was assigned as coming

from ASL located in the trapped lipid domain, and the short T_1 was assigned as an unresolved signal coming from ASL located in the bulk domain plus the purported CBD. For cortical and nuclear intact membrane and samples equilibrated with the air/N_2 mixture, SR signals were also successfully fitted to double exponentials (data not shown). Forcing the program to fit these results to triple-exponential curves did not improve the fitting (see Sect. 2.3 for explanation). The data from fitting the SR signals to the double exponentials for cortical and nuclear intact membranes equilibrated with different oxygen partial pressures (different % of air in gas mixture) were allowed to obtain time constants for the trapped lipid domain, which were further used for triple-exponential fittings.

As described in Sect. 1.1 and schematically shown in Fig. 2C, to "help" the fitting program fit SR signals to triple exponentials, we fixed time constants obtained for the trapped lipid domain from the double-exponential fittings for samples equilibrated with different oxygen partial pressures and again fitted these SR signals to triple exponentials. The representative SR signal and the fitting curve for the intact cortical membranes equilibrated with 30% air and with the fixed time constant for trapped lipids are shown in Fig. 3A. In this case, the SR signal can be fitted only to the double exponential with the fixed T_1 value for trapped lipids and the very similar T_1 value for the bulk lipids plus purported CBD as obtained from the double-exponential fit (without fixing the time constants for trapped lipids). The data from these measurements for cortical intact membranes equilibrated with different oxygen partial pressures are presented in Fig. 3B. These results indicate that only two domains are present in cortical intact membranes, namely trapped lipids and bulk lipids. The results are not surprising because CBDs were not present in cortical LLMs (Fig. 1C), so we did not expect to see CBDs in cortical intact membranes either (Fig. 1A).

The representative SR signal and the fitting curve for intact nuclear membranes equilibrated with 30% air and with the fixed time constant for trapped lipids is shown in Fig. 4A. In this case, the SR signal can be successfully fitted to the triple exponential with the fixed T_1 value for trapped lipids and two T_1 values for the bulk lipids and the CBD. The data from these measurements for nuclear intact membranes equilibrated with different oxygen partial pressures are presented in Fig. 4B. Based on this figure, three OTP values were calculated, indicating the presence of three domains in intact nuclear membranes. Comparison of these data with those obtained previously for nuclear LLMs (Mainali et al., 2012) allowed us to assign results to certain membrane domains, namely trapped lipids, bulk lipids, and the CBD. As indicated in Fig. 4B, in addition to the fixed OTP from trapped lipids, the new greater OTP value was assigned to bulk lipids and the new smaller value of the OTP to the CBD. For nuclear membranes, the CBD was present in LLMs (Fig. 1D), so we also expected to detect CBD in intact nuclear membranes (Fig. 1B).

We have successfully achieved the major goals that are indicated at the beginning of this section. We modified the DOT method to the new stage, which allowed the SR data for intact fiber cell membranes to be fitted to triple exponentials and detected the CBD in these membranes. We also showed that when the Chol content in fiber cell membranes is too low, as in the case of cortical membranes of two-year-old porcine lenses, the CBD is not observed in either the LLMs or intact membranes. However, when the Chol content is high

enough to induce the formation of CBDs in LLMs, like in the case of the nuclear membranes of two-year-old porcine lenses, the CBD is also observed in intact nuclear membranes.

3.2. Validation of the method

To validate this new approach, we focused on three points. First, we wanted to confirm that the obtained results are stable and independent of the recording/analysis conditions. Second, we wanted to evaluate the scattering of the results coming from preparation/technique sources. Third, and most significantly, we wanted to confirm that the third component in the SR signal is not an artifact but that it indicates the presence of the CBD in intact membranes.

The fitting of SR signals for nuclear membranes equilibrated with different oxygen partial pressures and fixed T_1 values for trapped lipids to triple-exponential functions gives stable, reliable, independent results on the recording (time increment, pulse power, and observing power) and simulation conditions (number of beginning points removed). Without fixing the T_1 value for trapped lipids, the fitting of SR signals to triple-exponential function was not reliable (see Sect. 2.3). This validates the stability of the proposed approach.

To perform statistical analysis, results were compared for six independently (separately) obtained cortical and six nuclear membrane samples from porcine lenses. It was assumed that the sample-to-sample differences were minimal because all animals were two years old and porcine lenses were obtained from the same meat factory and at the same time of the year. Thus, the scattering of the obtained data was the result of preparation/technique-related changes. The cumulative results for measured OTPs in domains in cortical and nuclear intact membranes are presented in Fig. 5A and 5B, respectively. Mean values and standard deviations for OTPs are indicated. Because our focus is on the CBD, statistical analysis (Student's *t*-test) of the data, which allowed determination of the statistically significant separations of mean values with P 0.05 (indicated by dashed lines in Fig. 5B), was performed only for nuclear intact membranes. The OTP values in the CBD have to be separated by $0.02\ \mu s^{-1}$, in the bulk domain by $0.46\ \mu s^{-1}$, and in the trapped lipids by $0.02\ \mu s^{-1}$ to be considered statistically significant. Greater separations indicate that differences came from sources other than preparation/technique. We can immediately conclude that separations of OTPs for three domains discriminated in the membranes of the porcine nucleus are statistically significant.

Human single lenses are connected with the unique health history of the donor. Thus, it is significant to separate changes due different health histories from those due to preparation/ technique factors. Procedures connected with preparations and measurements performed for human lenses are the same as for porcine lenses, which allowed us to assume that the scattering of the data from preparation/technique factors should be the same. Therefore, the values obtained here were used to compare the OTPs obtained for lenses of different human donors (Sect. 2.3).

Here, we use the OTP (which is proportional to the local oxygen diffusion-concentration product [see Eq. 1]) as the characteristic property of the CBD and other PL domain in LLMs and in intact fiber cell membranes. Extrapolation of the data in Fig. 4B to 100% air (notice that the spin-lattice relaxation rate $[T_1^{-1}]$ is plotted as a function of air in gas mixture)

allowed us to evaluate OTP values for the long T_1 component (which we assigned to the trapped lipid domain) and for two new components discriminated in the presence of oxygen from the short T_1 component of the SR signal in deoxygenated membranes. As indicated in Sect. 1.1 and schematically in Fig. 2C, these two components describe the OTPs in the bulk PL domain surrounding the CBD and in the CBD. The greater OTP is observed in the bulk PL domain and the smaller in the CBD.

Figure 5 contains cumulative values of the OTP obtained from fitting the SR signals to the triple-exponential functions for six porcine samples. In cortical membranes, the values obtained for the OTP in the bulk domain from triple- and double-exponential fittings were practically the same (see Fig. 5A). The third exponential was "neglected" by the fitting program; that is, its contribution (pre-exponential coefficient) was negligible (less than 1% of the total SR signal). The results were very different for nuclear membranes (Fig. 5B). Fitting SR signals to triple exponentials revealed new components in SR signals for samples equilibrated with air. We assigned these components as coming from the bulk lipid domain and from the CBD. Of course, the third component coming from the trapped lipid domain was fixed.

Due to the low Chol content, the two-year-old porcine cortical LLMs contain only one domain (the bulk domain), which is characterized by one value of the OTP (indicated in the caption to Fig. 5). Because of the high Chol content, nuclear LLMs contain two domains— the bulk domain and the CBD—and two values of the OTP are observed in these membranes (indicated in the caption to Fig. 5). The OTP values observed in bulk domains of cortical and nuclear LLMs are practically the same and in agreement with our observation that OTP values for PL membranes saturated with Chol are similar, independent of PL composition (Mainali et al., 2012, 2017b). The OTP value measured in the CBD of nuclear LLMs is close to that observed previously for the CBDs in model membranes (Mainali et al., 2013b; Raguz et al., 2011a, b).

Comparison of the OTP values obtained for cortical LLMs and cortical intact membranes (Fig. 5A) confirms that the data in intact membranes are assigned to those coming from ASL located in trapped lipids (the domain is not present in LLMs) and those coming from ASL located in the bulk domain (the entire cortical LLM forms the bulk domain). The effects of integral membrane proteins on the OTP value in the bulk domain sensed by ASL in intact membranes is small (as shown in Fig. 5A) because ASL is substantially excluded from the boundary lipid layer around these proteins (Bieri and Wallach, 1975; Warren et al., 1975), and the ASL located in trapped lipid domains does not contribute to the OTP measured in bulk lipids because of the small exchange rate of lipids between these domains (Kawasaki et al., 2001).

Comparison of the OTP values obtained for nuclear LLMs and nuclear intact membranes from triple-exponential fittings (Fig. 5B) confirms that the data in intact membranes are assigned to those coming from ASL located in trapped lipids (the domain is not present in LLMs) and those coming from ASL located in the bulk domain and in the CBD (both domains are present in nuclear LLMs). The OTP values in CBDs detected in LLMs and in intact membranes are very similar, although in intact membranes they are somewhat greater.

Also, the OTP values in the bulk domain observed in LLMs and in intact membranes are close. Fitting SR signals to triple-exponential functions increases the standard deviations of measured values, which are especially strong for the shortest T_1 component (see Sect. 2.3). Nevertheless, this comparison supports the assignment of measured values to certain membrane domains. Thus, the new approach can be used to detect CBDs in intact membranes. Data presented in Fig. 5 also support our hypothesis that CBDs exist in intact lens membranes only when they are also detected in LLMs.

3.3. CBDs can be detected in human cortical and nuclear intact fiber cell plasma membranes

We applied the new SR EPR spin-labeling approach to detect CBDs in human intact fiber cell plasma membranes from donors of different ages. Because the sensitivity of our SR EPR spectrometer allows us to perform experiments with samples prepared from a single lens, we were able to make separate measurements for the left and the right eyes of the same donor. As indicated in Sect. 2.2, we isolated fiber cell plasma membranes separately from lens cortices and nuclei for left and right eyes.

The representative set of data and a description of the analysis for cortical and nuclear membranes from the right eye lens of the 53-year-old donor are presented in Fig. 6. In that analysis, we followed the steps described in Sect. 1.1 and illustrated in Fig. 2B and 2C. The double-exponential fitting was used to obtain T_1 values of ASL in the trapped lipid domain at different oxygen partial pressures. Fig. 6A and 6B presents the results of the SR data analyzed using the triple-exponential fitting approach with the fixed T_1 value obtained for the trapped lipid domain from the double-exponential fittings. Using this approach, the unresolved data for the bulk domain plus CBD was split into two values, those coming from the bulk domain and those coming from the CBD. Extrapolation of these data to 100% air allowed evaluation of the OTP values in trapped lipids (fixed after the double-exponential fitting), in the bulk domain and in the CBD (appropriately indicated in Fig. 6). This type of measurements was performed for the right and the left eyes of 40-, 46-, and 53-year-old donors. The final OTP value results evaluated in different domains of fiber cell plasma membranes are presented in Fig. 7.

When measured in all three discriminated membrane domains in the right and left eye lenses of the same donor, the OTP value differences are negligible (not statistically significant), both in cortical and nuclear membranes. The only measured difference that slightly exceeded the allowed value of 0.21 μs^{-1} was that for the CBD in nuclear membranes of the 46-year-old donor, which had a value of 0.28 μs^{-1}. This is in agreement with the health history of the donors (obtained from the eye bank), which did not indicate any differences between eyes. Also, the differences from donor to donor were, in principle, not statistically significant, possibly because all lenses were clear, and the age differences were small, 13 years or less. We want to indicate two exceptions to this statement. The differences between the OTP measured in the bulk domain of the right eye of 40- and 46-year-old donors in cortical membranes and that measured in the right eye of 40- and 53-year-old donors in nuclear membranes are 0.59 μs^{-1} and 0.79 μs^{-1}, respectively, as compared with the allowed value of 0.46 μs^{-1} (see Sect.3.2). For each donor and all domains, the OTP value measured

in cortical membranes was somewhat greater than that measured in nuclear membranes. However, this difference was not statistically significant. Instead, we can discuss the trend. A trend, which is clearer for nuclear membranes, is the increase of the OTP in bulk domains and the decrease of the OTP in CBDs observed with the increased age of the donor.

The OTP values for CBDs in intact human membranes can only be compared with existing data for human LLMs (Mainali et al., 2017b). The OTP measured in intact membranes in CBDs (1.30 to 1.51 μs^{-1} for cortical membranes and 0.97 to 1.25 μs^{-1} for nuclear membranes) is significantly greater than that measured in LLMs from donors of the appropriate age group (0.8 μs^{-1} and 0.6 μs^{-1} in cortical and nuclear LLMs, respectively). The CBD is a pure Chol bilayer domain and should exhibit properties independent of those (composition, organization) of the surrounding bulk membrane. The significant factor that can affect the properties of the CBD is the size of the domain. Thus, the above results can be explained as the effect of the interface between the bulk domain and the CBD on the total (averaged) property of the CBD. In small CBDs, the interface occupies a large part of the domain and the effect of the surrounding bulk domain on the property of the CBD is significant (OTP values in the interface should be close to those in the bulk domain, ~4 μs^{-1}). When the size of the CBD increases, the effect of the interface becomes negligible and the OTP value becomes as low as ~0.6 μs^{-1}. Two major factors that should determine the size of CBDs in intact membranes are the Chol content (this factor also determines the size of the CBDs in LLMs) and the density and organization of integral membrane proteins (an additional factor observed in intact membranes). An increase in the Chol content should increase the size of the CBDs (as observed in LLMs (Mainali et al., 2017b)). However, larger OTP values observed in intact membranes as compared with those observed in appropriate LLMs indicate the strong effect of integral membrane proteins on the size of CBDs in intact membranes. Integral membrane proteins decrease the size of CBDs.

Now, with the use of the triple-exponential approach, we can measure OTP values in bulk domains without contamination from CBDs (Fig. 6A and 6B). This was not possible with the double-exponential approach, which allowed us to obtain only unresolved values of the OTP for the bulk domain plus the CBD.

4. Concluding Remarks

Although, CBCs were discriminated in model membranes with high Chol content, including LLMs, they were not detected in intact membranes of the eye lens fiber cell. There are two possible reasons for this. First, it is possible that CBDs do not exist in intact membranes. Second, existing methods, because of the presence of other domains in intact membranes, could not discriminated CBDs. Our measurements (Mainali et al., 2013b; Raguz et al., 2011a, b) and data from the literature (Jacob et al., 2013; Jacob and Mason, 2005; Jin et al., 2018; Litz et al., 2016) indicate that, in model membranes, when the Chol content is close to or exceeds the Chol solubility threshold in PL bilayers, CBDs are always present. Additionally, the formation of CBDs precedes the formation of Chol crystals (Mainali et al., 2013b). It is even suggested that CBDs form the precursors of Chol crystals (Mainali et al., 2015; Mason and Jacob, 2003). CBDs were detected in LLMs prepared from the total lipid extracts from intact fiber cell membranes. However, they were detected only when Chol

content in these membranes was high, greater than ~50 mol% (Mainali et al., 2013a, 2015). The fiber cell plasma membranes of human eye lenses are loaded with Chol with concentrations exceeding 50 mol% (Mainali et al., 2013a, 2015). In lenses from aged donors, the Chol content even exceeds the Chol solubility threshold (Jacob et al., 1999, 2001; Mainali et al., 2015). In these cases, Chol crystals are detected in human lenses. These results indicate that Chol content in intact human fiber cell plasma membranes is high enough to form CBDs in the lipid bilayer portion of these membranes. Thus, we directed our efforts to modifying existing methods for discriminating domains in intact membranes, so that we could discriminate CBDs if they exist in intact membranes.

Our methods for discriminating membrane domains use EPR spin-labeling techniques. Because the CBD is a pure Chol bilayer, it can be discriminated only with Chol analog spin labels, ASL and CSL. Both spin labels work well in model membranes (Mainali et al., 2013b; Raguz et al., 2011a, b). However, because of the very high hydrophobicity of CSL, intact membranes can be labeled only with ASL, and this spin label has been intensively used to investigate localizations and amounts of Chol in domains present in intact membranes (Mainali et al., 2017a; Mainali et al., 2012; Raguz et al., 2014, 2015b, c). Measurements with model membranes indicated that conventional EPR spectra and T_1s measured with ASL in CBDs and surrounding PLs are similar (almost identical) and indistinguishable by conventional and SR EPR approaches (Raguz et al., 2011a, b). Thus, the discrimination of the CBD from the surrounding bulk domain with ASL was only possible using the SR EPR DOT method (Subczynski et al., 2007). This approach was successful, but only to detect CBDs in model membranes (without integral membrane proteins). The DOT method is based on the dependence of oxygen solubility and diffusivity on the organization of membrane domains. Oxygen enhances spin-lattice relaxation and shortens T_1s. Its effect on T_1 in the CBD is significantly weaker than in bulk lipids, and the single-exponential SR signal (observed in the absence of oxygen) becomes the double exponential, where a faster component indicates OTP in bulk lipids and a slower component indicates OTP in the CBD (Raguz et al., 2011b). Fitting SR signals to double-exponential functions can easily be performed given reliable data. However, this is more complicated in intact membranes, because of the presence of membrane integral proteins. Integral proteins induce formation of other membrane domains (lipid environments) where ASL can be located. Our previous results showed that ASL can be located in the bulk domain and the purported CBD (formed in the lipid bilayer portion of intact membranes) and in trapped lipids (domain induced by the presence of integral proteins) (Mainali et al., 2012; Raguz et al., 2015c). Thus, we must fit the SR signal to the triple-exponential function in order to discriminate these domains. We were not successful in a straightforward fitting of SR signals to triple exponentials (see also Sect. 2.3). However, we were very successful when using an approach, we recently applied in a similar situation (Mainali et al., 2017a), namely fixing a few parameters before applying the triple-exponential fitting. Here, we fixed the relaxation characteristics of ASL coming from the trapped lipid domain obtained from the double-exponential fitting. This approach allowed us to split the unresolved SR signal coming from the bulk domain plus the CBD into two components coming separately from the bulk domain and from the CBD. That way, we showed that advanced DOT method allows

discrimination of the CBD in intact membranes where other lipid domains, induced by integral membrane proteins, are presented.

The obtained results increased our understanding of the organization and properties of the lipid bilayer portion of fiber cell plasma membranes. We now know that at a high Chol content pure CBDs are formed in the lipid bilayer portion of intact human fiber cell membranes. We have demonstrated that these domains can only be detected in intact membranes when they also are detected in model membranes prepared from the total lipid extracts from intact membranes. For intact eye lens fiber cell membranes from donors with transparent lenses, the differences between the properties (OTP) of CBDs in cortical and nuclear lens regions for the same donor were greater than those properties when compared between the same lens region, cortex or nucleus, of the left and the right eyes. As discussed previously for LLMs (Mainali et al., 2017b), the value of the OTP measured with ASL in the CBD is determined by the Chol content in these membranes and can determine the size of the individual CBD. The smaller the OTP, the greater the size of the CBD. We should mention that the Chol content also determines the amount of Chol involved in the formation of CBDs (the membrane surface occupied by CBDs). Thus, it can be concluded that CBDs occupy a greater area of the lipid bilayer portion in nuclear intact membranes than in cortical intact membranes. (Chol content in nuclear membranes is greater than in cortical membranes.) Also, the size of individual domains in nuclear membranes is greater than that in cortical membranes. (The OTP values in CBDs in nuclear membranes are smaller than those in cortical membranes.) Comparison of OTP values in human intact membranes with those in appropriate LLMs supports the hypothesis that the presence of integral membrane proteins decreases the size of individual CBDs.

In our opinion, the most significant function of the CBD in lens biology is that this pure Chol bilayer, when present in the membrane, provides a buffering capacity for the Chol concentration in the surrounding PL bilayer, keeping it at a constant saturating level. As shown in many experiments (Mainali et al., 2012; 2013; 2015; 2017b), the saturating content of Chol keeps the bulk physical properties of the lipid bilayer consistent and independent of changes in the PL composition. Thus, the CBD plays a crucial role in maintaining the homeostasis of the lens membrane by providing stability and ensuring that the physical properties of the lipid bilayer surrounding the membrane integral proteins are consistent, independent of the enormous changes in phospholipid composition during aging. The saturating Chol content in fiber cell plasma membranes (provided by the presence of the CBD) ensures that the lipid bilayer portion of the intact fiber cell membrane provides a high hydrophobic barrier, which protects against the uncontrolled leaking of small polar molecules. Thus, in human lenses, the transport of polar molecules from fiber cell to fiber cell is tightly controlled by aquaporin-0 and connexins, the most abundant integral transmembrane proteins in human lens fiber cell membranes. Finally, a hypothetical high barrier to oxygen permeation located at plasma membranes of nuclear fiber cells should help maintain a low oxygen partial pressure in the lens nucleus, even at the very low oxygen consumption rate in this region. The CBD forms a major membrane barrier to oxygen transport into the lens center (Plesnar et al., 2018), and this barrier is significantly greater in the lens nucleus (presented results). Thus, CBDs help protect the lens against cataract development. We would like to conclude that the combination of the results obtained for

intact membranes with those obtained previously for LLMs advance our understanding of the role of high Chol content and CBDs in fiber cell plasma membranes in lens biology, aging, and/or cataract formation.

Acknowledgements

References

Ashikawa I, Yin J-J, Subczynski WK, Kouyama T, Hyde JS, Kusumi A, 1994 Molecular organization and dynamics in bacteriorhodopsin-rich reconstituted membranes: discrimination of lipid environments by the oxygen transport parameter using a pulse ESR spinlabeling technique. Biochemistry 33, 4947–4952. [PubMed: 8161556]

Bassnett S, Shi Y, Vrensen GF, 2011 Biological glass: structural determinants of eye lens transparency. Philos. Trans. Royal Soc. Lond. Ser. B Biol. Sci 366, 1250–1264.

Bieri VG, Wallach DF, 1975 Variations of lipid-protein interactions in erythrocyte ghosts as a function of temperature and pH in physiological and non-physiological ranges. A study using a paramagnetic quenching of protein fluorescence by nitroxide lipid analogues. Biochim. Biophys. Acta 406, 415–423. [PubMed: 241415]

Borchman D, Delamere NA, Cauley LA, Paterson CA, 1989 Studies on the distribution of cholesterol, phospholipid and protein in the human and bovine lens. Lens Eye Toxic Res. 6, 703–724. [PubMed: 2487279]

Cenedella RJ, 1996 Cholesterol and cataracts. Surv. Ophthalmol 40, 320–337. [PubMed: 8658343]

de Almeida RF, Fedorov A, Prieto M, 2003 Sphingomyelin/phosphatidylcholine/cholesterol phase diagram: boundaries and composition of lipid rafts. Biophys. J 85, 2406–2416. [PubMed: 14507704]

East JM, Melville D, Lee AG, 1985 Exchange rates and numbers of annular lipids for the calcium and magnesium ion dependent adenosinetriphosphatase. Biochemistry 24, 2615–2623. [PubMed: 2992571]

Edidin M, 2003 The state of lipid rafts: from model membranes to cells. Annu. Rev. Biophys. Biomol. Struct 32, 257–283. [PubMed: 12543707]

Gonen T, Cheng Y, Kistler J, Walz T, 2004 Aquaporin-0 membrane junctions form upon proteolytic cleavage. J. Mol. Biol 342, 1337–1345. [PubMed: 15351655]

Gonen T, Cheng Y, Sliz P, Hiroaki Y, Fujiyoshi Y, Harrison SC, Walz T, 2005 Lipidprotein interactions in double-layered two-dimensional AQP0 crystals. Nature 438, 633–638. [PubMed: 16319884]

Jacob RF, Aleo MD, Self-Medlin Y, Doshna CM, Mason RP, 2013 1,2-naphthoquinone stimulates lipid peroxidation and cholesterol domain formation in model membranes. Invest. Ophthalmol. Vis. Sci 54, 7189–7197. [PubMed: 24130176]

Jacob RF, Cenedella RJ, Mason RP, 1999 Direct evidence for immiscible cholesterol domains in human ocular lens fiber cell plasma membranes. J. Biol. Chem 274, 31613–31618. [PubMed: 10531368]

Jacob RF, Cenedella RJ, Mason RP, 2001 Evidence for distinct cholesterol domains in fiber cell membranes from cataractous human lenses. J. Biol. Chem 276, 13573–13578. [PubMed: 11278611]

Jacob RF, Mason RP, 2005 Lipid peroxidation induces cholesterol domain formation in model membranes. J. Biol. Chem 280, 39380–39387. [PubMed: 16195227]

Jin X, Dimitriadis EK, Liu Y, Combs CA, Chang J, Varsano N, Stempinski E, Flores R, Jackson SN, Muller L, Woods AS, Addadi L, Kruth HS, 2018 Macrophages Shed Excess Cholesterol in Unique Extracellular Structures Containing Cholesterol Microdomains. Arterioscler. Thromb. Vac. Biol 38, 1504–1518.

Kawasaki K, Yin J-J, Subczynski WK, Hyde JS, Kusumi A, 2001 Pulse EPR detection of lipid exchange between protein rich raft and bulk domains in the membrane: methodology development and its application to studies of influenza viral membrane. Biophys. J 80, 738–748. [PubMed: 11159441]

Kistler J, Bullivant S, 1980 Lens gap junctions and orthogonal arrays are unrelated. FEBS Lett. 111, 73–78. [PubMed: 7358167]

Kusumi A, Subczynski WK, Hyde JS, 1982 Oxygen transport parameter in membranes as deduced by saturation recovery measurements of spin-lattice relaxation times of spin labels. Proc. Natl. Acad. Sci. USA 79, 1854–1858. [PubMed: 6952236]

Li LK, Roy D, Spector A, 1986 Changes in lens protein in concentric fractions from individual normal human lenses. Curr. Eye Res 5, 127–135. [PubMed: 3956240]

Li LK, So L, Spector A, 1985 Membrane cholesterol and phospholipid in consecutive concentric sections of human lenses. J. Lipid Res 26, 600–609. [PubMed: 4020298]

Li LK, So L, Spector A, 1987 Age-dependent changes in the distribution and concentration of human lens cholesterol and phospholipids. Biochim. Biophys. Acta 917, 112–120. [PubMed: 3790601]

Litz JP, Thakkar N, Portet T, Keller SL, 2016 Depletion with Cyclodextrin Reveals Two Populations of Cholesterol in Model Lipid Membranes. Biophys. J 110, 635–645. [PubMed: 26840728]

Mainali L, Camenisch TG, Hyde JS, Subczynski WK, 2017a Saturation Recovery EPR Spin-Labeling Method for Quantification of Lipids in Biological Membrane Domains. Appl. Magn. Reson 48, 1355–1373. [PubMed: 29805201]

Mainali L, Raguz M, Camenisch TG, Hyde JS, Subczynski WK, 2011 Spin-label saturation-recovery EPR at W-band: applications to eye lens lipid membranes. J. Magn. Reson 212, 86–94. [PubMed: 21745756]

Mainali L, Raguz M, O'Brien WJ, Subczynski WK, 2012 Properties of fiber cell plasma membranes isolated from the cortex and nucleus of the porcine eye lens. Exp. Eye Res 97, 117129.

Mainali L, Raguz M, O'Brien WJ, Subczynski WK, 2013a Properties of membranes derived from the total lipids extracted from the human lens cortex and nucleus. Biochim. Biophys. Acta 1828, 1432–1440. [PubMed: 23438364]

Mainali L, Raguz M, O'Brien WJ, Subczynski WK, 2015 Properties of membranes derived from the total lipids extracted from clear and cataractous lenses of 61–70-year-old human donors. Eur. Biophys. J 44, 91–102. [PubMed: 25502634]

Mainali L, Raguz M, O'Brien WJ, Subczynski WK, 2017b. Changes in the Properties and Organization of Human Lens Lipid Membranes Occurring with Age. Curr. Eye Res 42, 721731.

Mainali L, Raguz M, Subczynski WK, 2013b Formation of Cholesterol Bilayer Domains Precedes Formation of Cholesterol Crystals in Cholesterol/Dimyristoylphosphatidylcholine Membranes: EPR and DSC Studies. J. Phys. Chem. B 117, 8994–9003. [PubMed: 23834375]

Marsh D, 1997 Stoichiometry of lipid-protein interaction and integral membrane protein structure. Eur. Biophys. J 26, 203–208.

Mason RP, Jacob RF, 2003 Membrane microdomains and vascular biology. Emerging role in atherogenesis. Circulation 107, 2270–2273. [PubMed: 12732593]

Mett RR, Sidabras JW, Hyde JS, 2007 Uniform radio frequency fields in loop-gap resonators for EPR spectroscopy. Appl. Magn. Reson 31, 573–589.

Plesnar E, Subczynski WK, Pasenkiewicz-Gierula M, 2013 Comparative Computer Simulation Study of Cholesterol in Hydrated Unary and Binary Lipid Bilayers and in an Anhydrous Crystal. J. Phys. Chem. B 117, 8758–8769. [PubMed: 23848956]

Plesnar E, Szczelina R, Subczynski WK, Pasenkiewicz-Gierula M, 2018 Is the cholesterol bilayer domain a barrier to oxygen transport into the eye lens? Biochim. Biophys. Acta 1860, 434–441.

Raguz M, Ilic N, Kumar S, Zereba M, Mainali L, Subczynski WK, 2015a Cholesterol Bilayer Domain in Phospholipid Bilayer Membranes can be Detected by Confocal Microscope. Biophys. J 108, 403a–404a.

Raguz M, Mainali L, O'Brien WJ, Subczynski WK, 2014 Lipid-protein interactions in plasma membranes of fiber cells isolated from the human eye lens. Exp. Eye Res 120, 138–151. [PubMed: 24486794]

Raguz M, Mainali L, O'Brien WJ, Subczynski WK, 2015b Amounts of phospholipids and cholesterol in lipid domains formed in intact lens membranes: Methodology development and its application to studies of porcine lens membranes. Exp. Eye Res 140, 179–186. [PubMed: 26384651]

Raguz M, Mainali L, O'Brien WJ, Subczynski WK, 2015c Lipid domains in intact fibercell plasma membranes isolated from cortical and nuclear regions of human eye lenses of donors from different age groups. Exp. Eye Res 132, 78–90. [PubMed: 25617680]

Raguz M, Mainali L, Widomska J, Subczynski WK, 2011a The immiscible cholesterol bilayer domain exists as an integral part of phospholipid bilayer membranes. Biochim. Biophys. Acta 1808, 1072–1080. [PubMed: 21192917]

Raguz M, Mainali L, Widomska J, Subczynski WK, 2011b Using spin-label electron paramagnetic resonance (EPR) to discriminate and characterize the cholesterol bilayer domain. Chem. Phys. Lipids 164, 819–829. [PubMed: 21855534]

Raguz M, Widomska J, Dillon J, Gaillard ER, Subczynski WK, 2009 Physical properties of the lipid bilayer membrane made of cortical and nuclear bovine lens lipids: EPR spin-labeling studies. Biochim. Biophys. Acta 1788, 2380–2388. [PubMed: 19761756]

Rog T, Vattulainen I, 2014 Cholesterol, sphingolipids, and glycolipids: what do we know about their role in raft-like membranes? Chem. Phys. Lipids 184, 82–104. [PubMed: 25444976]

Rujoi M, Jin J, Borchman D, Tang D, Yappert MC, 2003 Isolation and lipid characterization of cholesterol-enriched fractions in cortical and nuclear human lens fibers. Invest. Ophthalmol. Vis. Sci 44, 1634–1642. [PubMed: 12657603]

Ryba NJ, Horvath LI, Watts A, Marsh D, 1987 Molecular exchange at the lipid-rhodopsin interface: spin-label electron spin resonance studies of rhodopsin-dimyristoylphosphatidylcholine recombinants. Biochemistry 26, 3234–3240. [PubMed: 3038180]

Sidabras JW, Sarna T, Mett RR, Hyde JS, 2017 Uniform field loop-gap resonator and rectangular TEU02 for aqueous sample EPR at 94GHz. J. Magn. Reson 282, 129–135. [PubMed: 28803092]

Simons K, Vaz WL, 2004 Model systems, lipid rafts, and cell membranes. Rev. Biophys. Biomol. Struct 33, 269–295.

Subczynski WK, Felix CC, Klug CS, Hyde JS, 2005 Concentration by centrifugation for gas exchange EPR oximetry measurements with loop-gap resonators. J. Magn. Reson 176, 244248.

Subczynski WK, Mainali L, Raguz M, O'Brien WJ, 2017 Organization of lipids in fibercell plasma membranes of the eye lens. Exp. Eye Res 156, 79–86. [PubMed: 26988627]

Subczynski WK, Widomska J, Wisniewska A, Kusumi A, 2007 Saturation-recovery electron paramagnetic resonance discrimination by oxygen transport (DOT) method for characterizing membrane domains, Methods in Molecular Biology, Lipid Rafts McIntosh TJ, ed. ed. Humana Press, Totowa, pp. 143–157.

Veatch SL, Keller SL, 2003 A closer look at the canonical 'Raft Mixture' in model membrane studies. Biophys. J 84, 725–726. [PubMed: 12524324]

Warren GB, Houslay MD, Metcalfe JC, Birdsall NJ, 1975 Cholesterol is excluded from the phospholipid annulus surrounding an active calcium transport protein. Nature 255, 684–687. [PubMed: 124402]

Zelenka PS, 1984 Lens lipids. Curr. Eye Res 3, 1337–1359. [PubMed: 6391828]
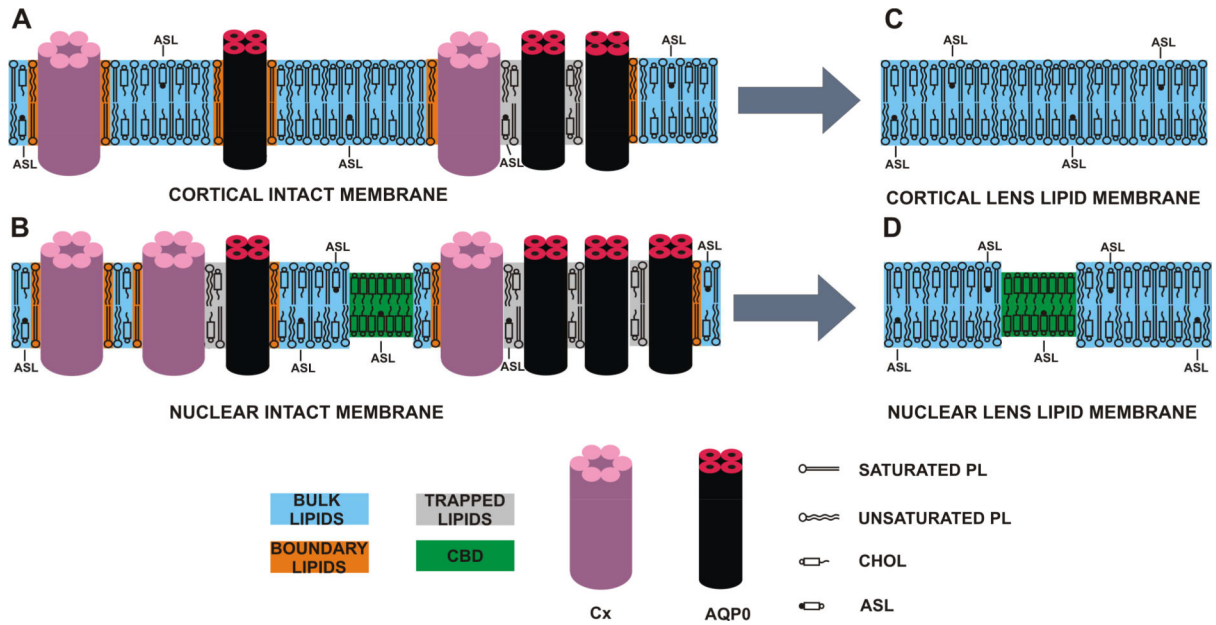
Highlights

Cholesterol bilayer domain (CBDs) have been detected in intact biological membranes

CBDs were detected in intact membranes when the cholesterol content was high enough

CBDs were detected in both cortical and nuclear human fiber-cell eye lens membranes

Fig. 1.
Schematic drawing of the intact (A and B) and the LLM (C and D) porcine cortical (A and C) and nuclear (B and C) membranes. Lipid domains induced by the high Chol content and the presence of integral membrane proteins (mainly connexins [Cx] and aquaporins [AQPO]) are indicated. Chol analog ASL is distributed between the CBD, bulk lipids, and trapped lipids. Note that Chol as well as ASL are excluded from boundary lipids. The nitroxide moiety of ASL is indicated by the black dot. Cortical LLMs (C) are formed by bulk lipids and do not contain CBDs. CBDs are not expected in cortical intact membranes (A). Nuclear LLMs are formed by coexisting bulk lipids and CBDs (D). CBDs are also expected to be present in nuclear intact membranes (B).
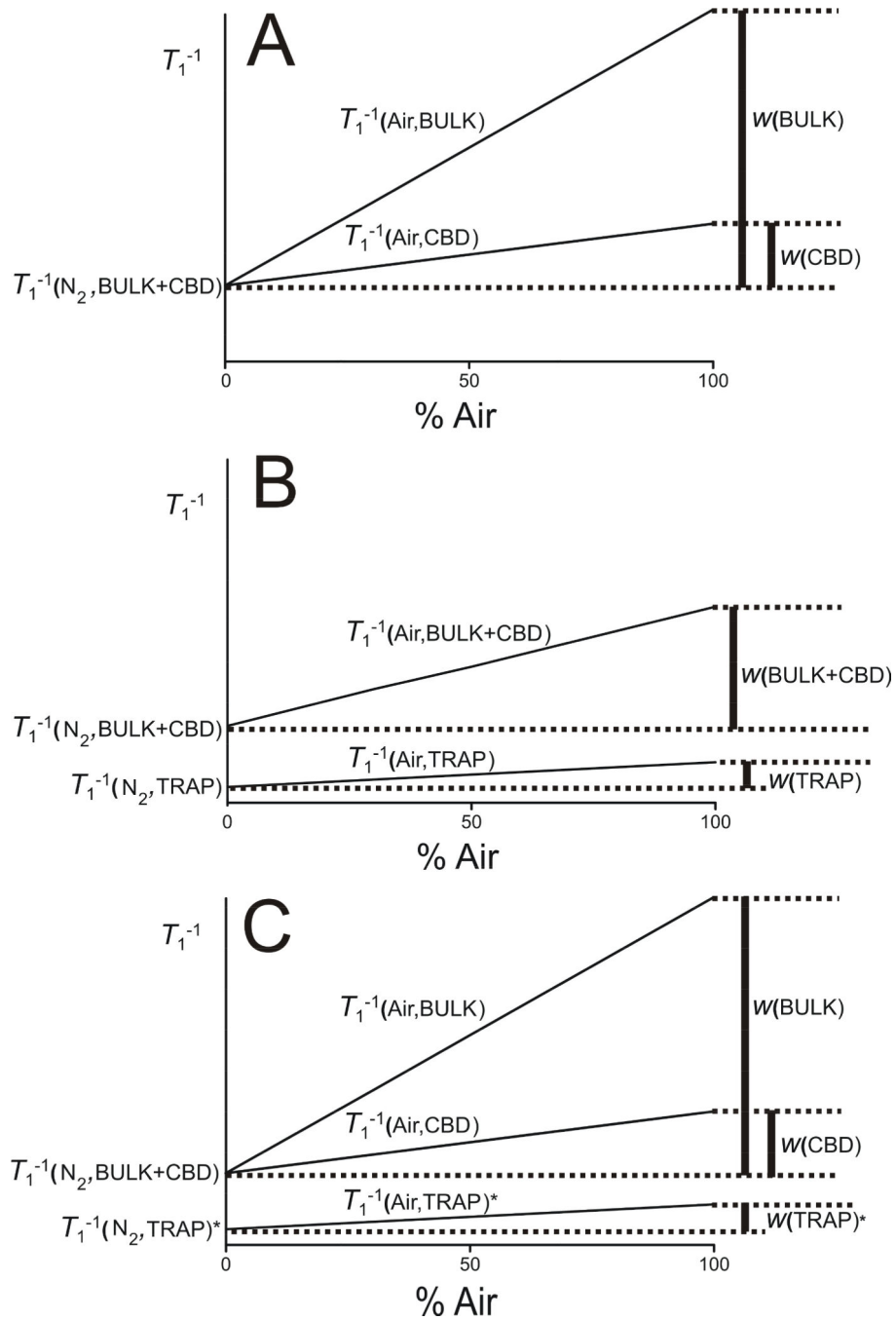
Fig. 2.
(A) Schematic illustration of the procedure for processing the SR signal fitting data from ASL in LLMs containing CBDs to double-exponential functions. This procedure is described by Eqs. 2 and 3. (B) Schematic illustration of the procedure for processing the SR signal fitting data from ASL in intact fiber cell membranes containing CBDs to double-exponential functions. This procedure is described by Eqs. 4 and 5. (C) Schematic illustration of the procedure for processing the data from fitting the SR signals from ASL in

intact fiber cell membranes containing CBDs to triple-exponential functions. This procedure is described by Eqs. 6, 7, and 8. For detailed information, see Sect. 1.1.
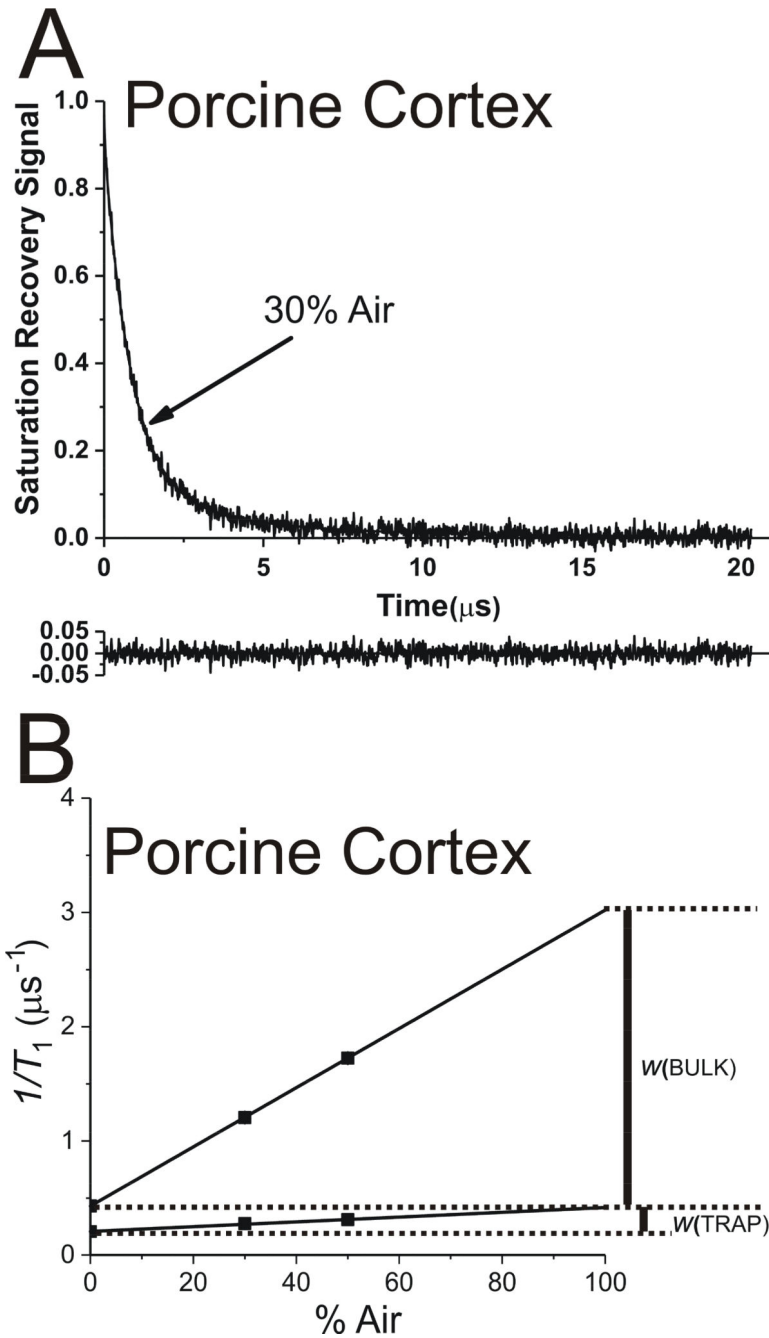
Fig. 3.

The representative SR signal of ASL in cortical fiber cell plasma membranes from porcine eye lenses equilibrated with an air/N_2 gas mixture containing 30% air. This signal can be successfully fitted only with a double-exponential function with time constants of 3.9 ± 0.28 µs and 0.80 ± 0.02 µs (data not shown). When the triple-exponential fitting program was applied, with the fixed longest time constant (3.9^* µs) (A), only two reliable time constants were obtained ($3.9^* \pm 0.25$ µs and 0.83 ± 0.01 µs, which were practically the same as for double-exponential fitting). The contribution of the third component was negligible. Additionally, it was characterized by the time constant, which has no meaning for the

investigated system. These suggest that only two components were present in the SR signal. The residual, shown at the bottom, indicates the goodness of the fit. The SR signal fitting data obtained for intact cortical membranes equilibrated with different oxygen partial pressures (different % of air in gas mixture) to triple exponentials (B) are plotted as a function of air in gas mixture. The double-exponential fitting for samples at different oxygen partial pressures (data not shown) is used to obtain T_1 values for ASL in the trapped lipid domain. These fixed values are further used to fit the data to triple-exponential functions (B). Note that the spin-lattice relaxation rate (T_1^{-1}) is used in these plots. As indicated above, SR signals can be fitted only to double-exponential functions discriminating only two lipid domains in cortical intact membranes. The extrapolation of the data to 100% air allows evaluation of the OTP values in discriminated domains.
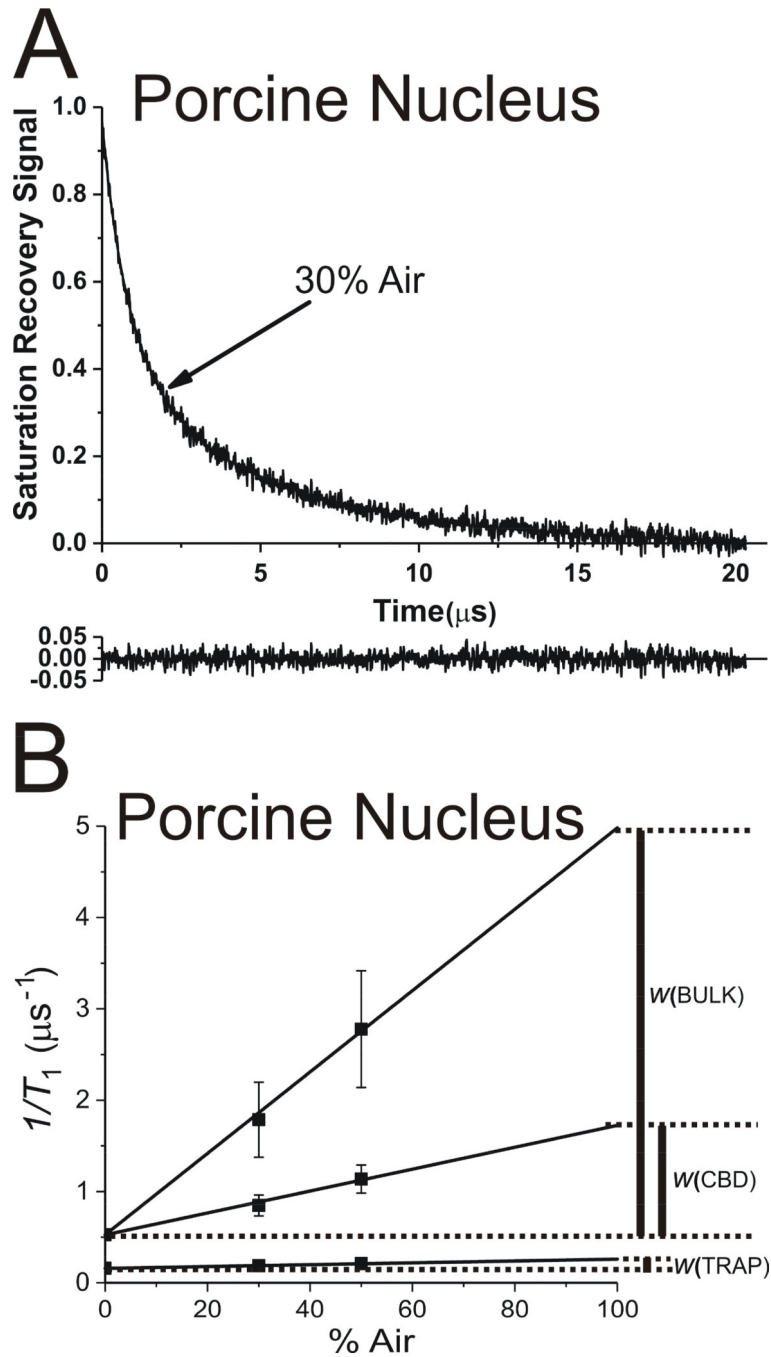
Fig. 4.

The representative SR signal of ASL in nuclear fiber cell plasma membranes from porcine eye lenses equilibrated with an air/N_2 gas mixture containing 30% air. This signal can be successfully fitted with a double-exponential function with time constants of 5.43 ± 0.13 μs and 0.96 ± 0.03 μs (data not shown) and with a triple-exponential function with time constants of $5.43^* \pm 0.13$ μs, 1.18 ± 0.16 μs, and 0.56 ± 0.13 μs (A). The reliable fit to a triple-exponential function was possible only when the longest time constant for the fitting (5.43^* μs) was taken from the double-exponential fit and fixed. The residual, shown at the

bottom, indicates the goodness of the fit. The SR signal fitting data obtained for intact nuclear membranes equilibrated with different oxygen partial pressures (different % of air in gas mixture) to triple exponentials (B) are plotted as a function of air in gas mixture. The double-exponential fitting for samples at different oxygen partial pressures (data not shown) is used to obtain T_1 values for ASL in the trapped lipid domain. These fixed values are further used to fit the data to triple-exponential functions (B). Note that the spin-lattice relaxation rate (T_1^{-1}) is used in these plots. The extrapolation of the data to 100% air allows evaluation of the OTP values in discriminated domains.
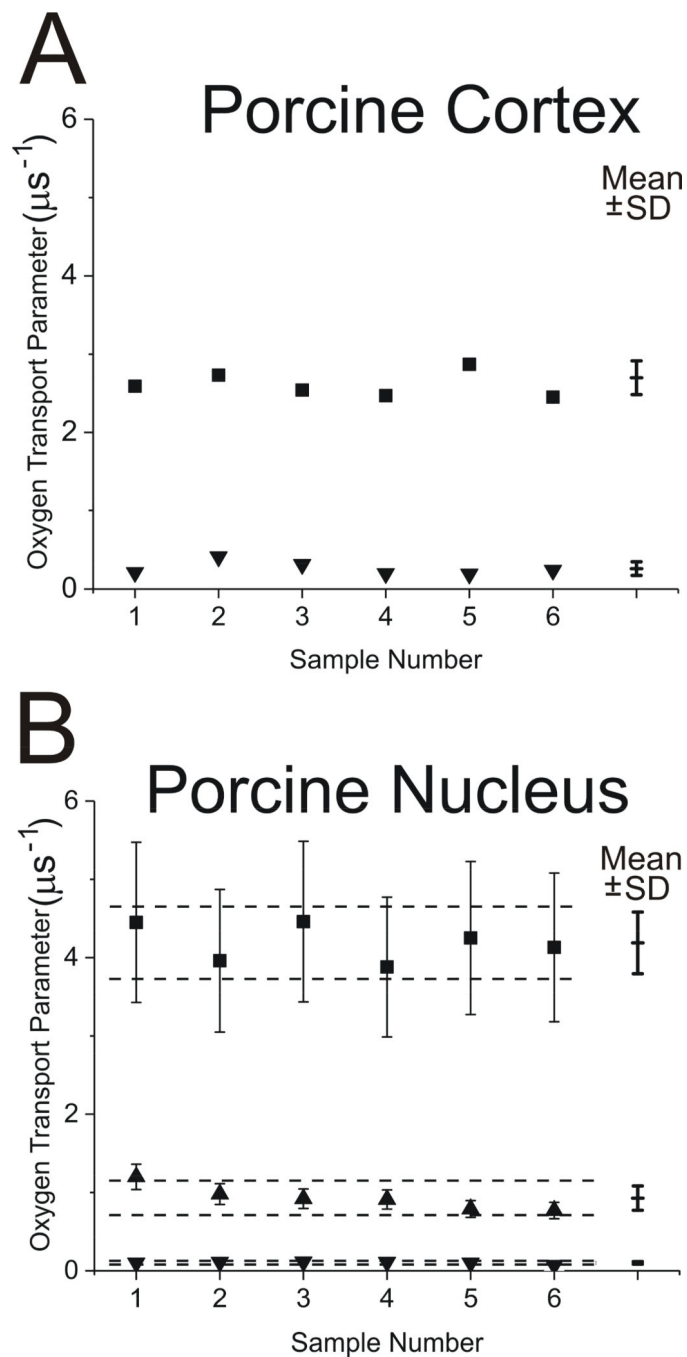
Fig. 5.
The OTP measured with ASL in domains discriminated in cortical (A) and nuclear (B) intact fiber cell membrane samples obtained separately from porcine eye lenses. Symbols are as follows: ▲ - CBD; ■ - bulk domain; ▼ - trapped lipids. Mean values (Mean) and standard deviations (SD) obtained from triple-exponential fits for each group are indicated. Dashed lines indicate the interval around the mean values outside of which the differences between means are statistically significant (P 0.05). These results were obtained based on the analysis of SR signals for ASL as indicated in Figs. 3B and 4B. The value of the OTP in the

bulk domain of the cortical LLMs is 2.85 μs^{-1}, and the values of the OTP in the bulk domain and in the CBD of the nuclear LLMs are 3.0 and 0.52 μs^{-1}, respectively.
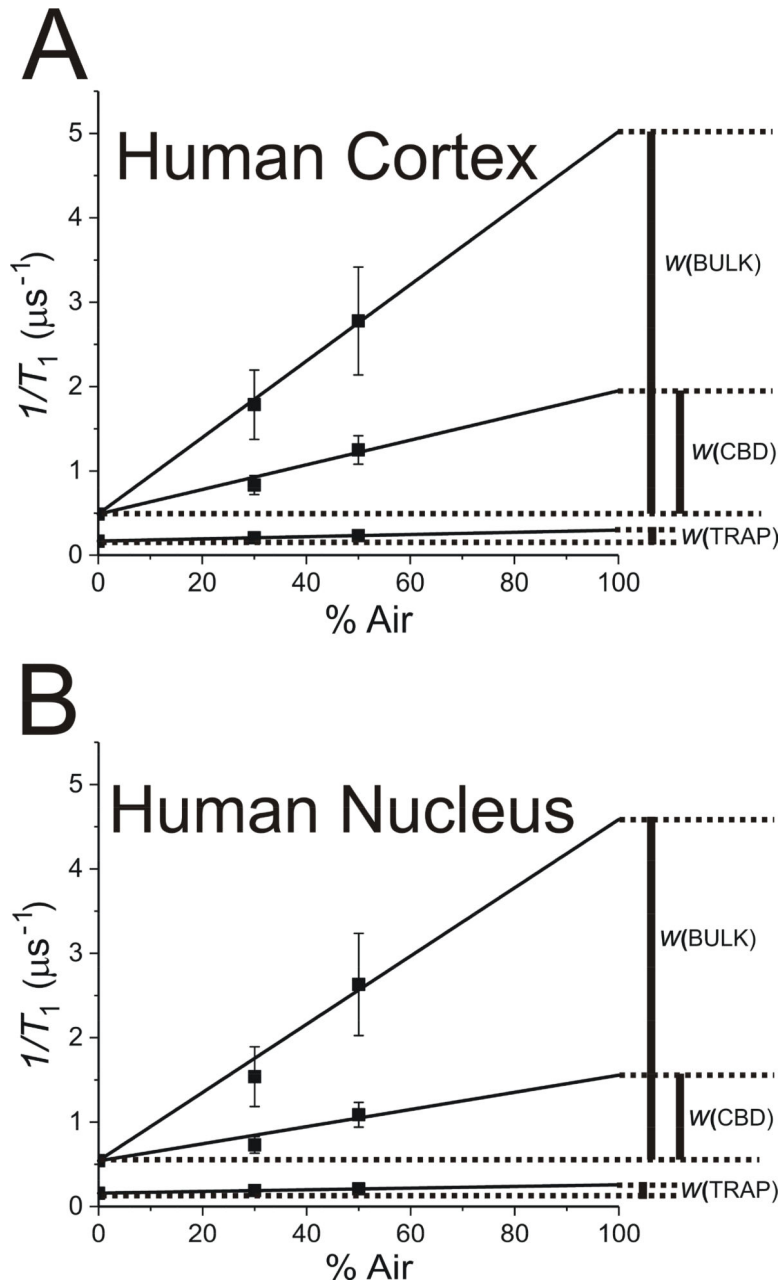
Fig. 6.
Representative set of data obtained from the SR signal fitting of ASL in cortical (A) and nuclear (B) fiber cell plasma membranes from the lens of the right eye of a 53-year-old human donor. The results were obtained from triple-exponential fits. Here, the spin-lattice relaxation rate (T_1^{-1}) is plotted as a function of air in gas mixture with which samples were equilibrated. The double-exponential fitting for samples at different oxygen partial pressures (data not shown) is used to obtain T_1 values for ASL in the trapped lipid domain. These fixed values are further used to fit the data to triple-exponential functions (A and B). The extrapolation of the data to 100% air allows evaluation of the OTP values in discriminated domains.
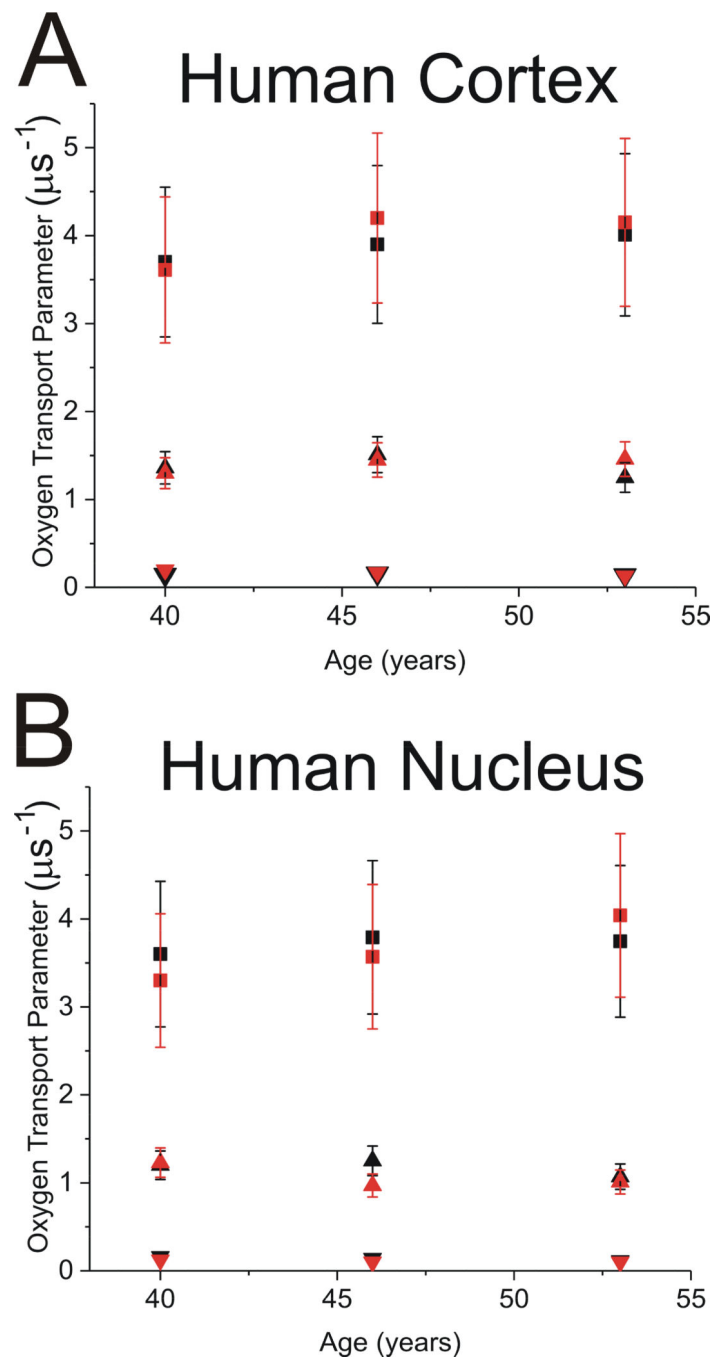
Fig. 7.
The OTP measured with ASL in domains discriminated in cortical (A) and nuclear (B) intact fiber cell membranes obtained separately from left (black symbols) and right (red symbols) eye lenses of 40-, 46-, and 53-year-old human donors. Symbols indicating results for certain domains are the same as described in the Fig. 5 caption. The results were obtained from triple-exponential fits. In trapped lipids, the results from left and right eye lenses overlap.

These results were obtained based on the analysis of SR signals for ASL as indicated in Fig. 6.